

Fermi National Accelerator Laboratory

**FERMILAB Conf-96/258-E
DØ**

**Results from a Search for a Neutral Scalar
Produced in Association with a W Boson
in $p\bar{p}$ Collisions at $\sqrt{s} = 1.8$ TeV**

**S. Abachi et al.
The DØ Collaboration**

*Fermi National Accelerator Laboratory
P.O. Box 500, Batavia, Illinois 60510-0500*

August 1996

Submitted to the 28th International Conference on High Energy Physics, Warsaw, Poland, July 25-31, 1996.

Disclaimer

This report was prepared as an account of work sponsored by an agency of the United States Government. Neither the United States Government nor any agency thereof, nor any of their employees, makes any warranty, express or implied, or assumes any legal liability or responsibility for the accuracy, completeness or usefulness of any information, apparatus, product or process disclosed, or represents that its use would not infringe privately owned rights. Reference herein to any specific commercial product, process or service by trade name, trademark, manufacturer or otherwise, does not necessarily constitute or imply its endorsement, recommendation or favoring by the United States Government or any agency thereof. The views and opinions of authors expressed herein do not necessarily state or reflect those of the United States Government or any agency thereof.

Distribution

Approved for public release: further dissemination unlimited.

Results from a Search for a Neutral Scalar Produced in Association with a W Boson in $p\bar{p}$ Collisions at $\sqrt{s} = 1.8$ TeV.

The DØ Collaboration¹
(July 1996)

This paper presents a search for production of a hypothetical heavy particle X in association with a W boson. For the search presented here, the kinematics and acceptances are modelled under the assumption that the X particle has the spin and decay properties of the standard model Higgs boson with the modification that only $X \rightarrow b\bar{b}$ decays are allowed. The W is required to decay via either the electron or muon mode. The complete DØ 1992-1995 data set is used. This sample has an integrated luminosity of 100 pb^{-1} and was taken at a center-of-mass energy of 1.8 TeV. Limits are set on the number of associated production events and the production cross section.

S. Abachi,¹⁴ B. Abbott,²⁸ M. Abolins,²⁵ B.S. Acharya,⁴³ I. Adam,¹² D.L. Adams,³⁷ M. Adams,¹⁷
 S. Ahn,¹⁴ H. Aihara,²² J. Alitti,⁴⁰ G. Álvarez,¹⁸ G.A. Alves,¹⁰ E. Amidi,²⁹ N. Amos,²⁴
 E.W. Anderson,¹⁹ S.H. Aronson,⁴ R. Astur,⁴² R.E. Avery,³¹ M.M. Baarmand,⁴² A. Baden,²³
 V. Balamurali,³² J. Balderston,¹⁶ B. Baldin,¹⁴ S. Banerjee,⁴³ J. Bantly,⁵ J.F. Bartlett,¹⁴
 K. Bazizi,³⁹ J. Bendich,²² S.B. Beri,³⁴ I. Bertram,³⁷ V.A. Bezzubov,³⁵ P.C. Bhat,¹⁴
 V. Bhatnagar,³⁴ M. Bhattacharjee,¹³ A. Bischoff,⁹ N. Biswas,³² G. Blazey,¹⁴ S. Blessing,¹⁵
 P. Bloom,⁷ A. Boehnlein,¹⁴ N.I. Bojko,³⁵ F. Borcharding,¹⁴ J. Borders,³⁹ C. Boswell,⁹
 A. Brandt,¹⁴ R. Brock,²⁵ A. Bross,¹⁴ D. Buchholz,³¹ V.S. Burtovoi,³⁵ J.M. Butler,³
 W. Carvalho,¹⁰ D. Casey,³⁹ H. Castilla-Valdez,¹¹ D. Chakraborty,⁴² S.-M. Chang,²⁹
 S.V. Chekulaev,³⁵ L.-P. Chen,²² W. Chen,⁴² S. Choi,⁴¹ S. Chopra,²⁴ B.C. Choudhary,⁹
 J.H. Christenson,¹⁴ M. Chung,¹⁷ D. Claes,⁴² A.R. Clark,²² W.G. Cobau,²³ J. Cochran,⁹
 W.E. Cooper,¹⁴ C. Cretsinger,³⁹ D. Cullen-Vidal,⁵ M.A.C. Cummings,¹⁶ D. Cutts,⁵ O.I. Dahl,²²
 K. De,⁴⁴ M. Demarteau,¹⁴ N. Denisenko,¹⁴ D. Denisov,¹⁴ S.P. Denisov,³⁵ H.T. Diehl,¹⁴
 M. Diesburg,¹⁴ G. Di Loreto,²⁵ R. Dixon,¹⁴ P. Draper,⁴⁴ J. Drinkard,⁸ Y. Ducros,⁴⁰
 S.R. Dugad,⁴³ D. Edmunds,²⁵ J. Ellison,⁹ V.D. Elvira,⁴² R. Engelmann,⁴² S. Eno,²³ G. Eppley,³⁷
 P. Ermolov,²⁶ O.V. Eroshin,³⁵ V.N. Evdokimov,³⁵ S. Fahey,²⁵ T. Fahland,⁵ M. Fatyga,⁴
 M.K. Fatyga,³⁹ J. Featherly,⁴ S. Feher,¹⁴ D. Fein,² T. Ferbel,³⁹ G. Finocchiaro,⁴² H.E. Fisk,¹⁴
 Y. Fisysak,⁷ E. Flattum,²⁵ G.E. Forden,² M. Fortner,³⁰ K.C. Frame,²⁵ P. Franzini,¹² S. Fuess,¹⁴
 E. Gallas,⁴⁴ A.N. Galyaev,³⁵ T.L. Geld,²⁵ R.J. Genik II,²⁵ K. Genser,¹⁴ C.E. Gerber,¹⁴
 B. Gibbard,⁴ V. Glebov,³⁹ S. Glenn,⁷ J.F. Glicenstein,⁴⁰ B. Gobbi,³¹ M. Goforth,¹⁵
 A. Goldschmidt,²² B. Gómez,¹ G. Gomez,²³ P.I. Goncharov,³⁵ J.L. González Solís,¹¹ H. Gordon,⁴
 L.T. Goss,⁴⁵ N. Graf,⁴ P.D. Grannis,⁴² D.R. Green,¹⁴ J. Green,³⁰ H. Greenlee,¹⁴ G. Griffin,⁸
 N. Grossman,¹⁴ P. Grudberg,²² S. Grünendahl,³⁹ W.X. Gu,^{14,*} G. Guglielmo,³³ J.A. Guida,²

¹Submitted to the 28th International Conference on High Energy Physics, Warsaw, Poland, 25-31 July 1996.

- J.M. Guida,⁵ W. Guryan,⁴ S.N. Gurzhiev,³⁵ P. Gutierrez,³³ Y.E. Gutnikov,³⁵ N.J. Hadley,²³
 H. Haggerty,¹⁴ S. Hagopian,¹⁵ V. Hagopian,¹⁵ K.S. Hahn,³⁹ R.E. Hall,⁸ S. Hansen,¹⁴
 R. Hatcher,²⁵ J.M. Hauptman,¹⁹ D. Hedin,³⁰ A.P. Heinson,⁹ U. Heintz,¹⁴
 R. Hernández-Montoya,¹¹ T. Heuring,¹⁵ R. Hirosky,¹⁵ J.D. Hobbs,¹⁴ B. Hoeneisen,^{1,†}
 J.S. Hoftun,⁵ F. Hsieh,²⁴ Tao Hu,^{14,*} Ting Hu,⁴² Tong Hu,¹⁸ T. Huehn,⁹ S. Igarashi,¹⁴ A.S. Ito,¹⁴
 E. James,² J. Jaques,³² S.A. Jerger,²⁵ J.Z.-Y. Jiang,⁴² T. Joffe-Minor,³¹ H. Johari,²⁹ K. Johns,²
 M. Johnson,¹⁴ H. Johnstad,²⁹ A. Jonckheere,¹⁴ M. Jones,¹⁶ H. Jöstlein,¹⁴ S.Y. Jun,³¹
 C.K. Jung,⁴² S. Kahn,⁴ G. Kalbfleisch,³³ J.S. Kang,²⁰ R. Kehoe,³² M.L. Kelly,³² L. Kerth,²²
 C.L. Kim,²⁰ S.K. Kim,⁴¹ A. Klatchko,¹⁵ B. Klima,¹⁴ B.I. Klochkov,³⁵ C. Klopfenstein,⁷
 V.I. Klyukhin,³⁵ V.I. Kochetkov,³⁵ J.M. Kohli,³⁴ D. Koltick,³⁵ A.V. Kostritsky,³⁵ J. Kotcher,⁴
 J. Kourlas,²⁸ A.V. Kozelov,³⁵ E.A. Kozlovski,³⁵ M.R. Krishnaswamy,⁴³ S. Krzywdzinski,¹⁴
 S. Kunori,²³ S. Lami,⁴² G. Landsberg,¹⁴ J-F. Lebrat,⁴⁰ A. Leflat,²⁶ H. Li,⁴² J. Li,⁴⁴ Y.K. Li,³¹
 Q.Z. Li-Demarteau,¹⁴ J.G.R. Lima,³⁸ D. Lincoln,²⁴ S.L. Linn,¹⁵ J. Linnemann,²⁵ R. Lipton,¹⁴
 Y.C. Liu,³¹ F. Lobkowicz,³⁹ S.C. Loken,²² S. Lökös,⁴² L. Lueking,¹⁴ A.L. Lyon,²³
 A.K.A. Maciel,¹⁰ R.J. Madaras,²² R. Madden,¹⁵ L. Magaña-Mendoza,¹¹ S. Mani,⁷ H.S. Mao,^{14,*}
 R. Markeloff,³⁰ L. Markosky,² T. Marshall,¹⁸ M.I. Martin,¹⁴ B. May,³¹ A.A. Mayorov,³⁵
 R. McCarthy,⁴² T. McKibben,¹⁷ J. McKinley,²⁵ T. McMahon,³³ H.L. Melanson,¹⁴
 J.R.T. de Mello Neto,³⁸ K.W. Merritt,¹⁴ H. Miettinen,³⁷ A. Mincer,²⁸ J.M. de Miranda,¹⁰
 C.S. Mishra,¹⁴ N. Mokhov,¹⁴ N.K. Mondal,⁴³ H.E. Montgomery,¹⁴ P. Mooney,¹ H. da Motta,¹⁰
 M. Mudan,²⁸ C. Murphy,¹⁷ F. Nang,⁵ M. Narain,¹⁴ V.S. Narasimham,⁴³ A. Narayanan,²
 H.A. Neal,²⁴ J.P. Negret,¹ E. Neis,²⁴ P. Nemethy,²⁸ D. Nešić,⁵ M. Nicola,¹⁰ D. Norman,⁴⁵
 L. Oesch,²⁴ V. Oguri,³⁸ E. Oltman,²² N. Oshima,¹⁴ D. Owen,²⁵ P. Padley,³⁷ M. Pang,¹⁹
 A. Para,¹⁴ C.H. Park,¹⁴ Y.M. Park,²¹ R. Partridge,⁵ N. Parua,⁴³ M. Paterno,³⁹ J. Perkins,⁴⁴
 A. Peryshkin,¹⁴ M. Peters,¹⁵ H. Piekarz,¹⁵ Y. Pischalnikov,³⁵ V.M. Podstavkov,³⁵ B.G. Pope,²⁵
 H.B. Prosper,¹⁵ S. Protopopescu,⁴ D. Pušeljčić,²² J. Qian,²⁴ P.Z. Quintas,¹⁴ R. Raja,¹⁴
 S. Rajagopalan,⁴² O. Ramirez,¹⁷ M.V.S. Rao,⁴³ P.A. Rapidis,¹⁴ L. Rasmussen,⁴² S. Reucroft,²⁹
 M. Rijssenbeek,⁴² T. Rockwell,²⁵ N.A. Roe,²² P. Rubinov,³¹ R. Ruchti,³² J. Rutherford,²
 A. Sánchez-Hernández,¹¹ A. Santoro,¹⁰ L. Sawyer,⁴⁴ R.D. Schamberger,⁴² H. Schellman,³¹
 J. Sculli,²⁸ E. Shabalina,²⁶ C. Shaffer,¹⁵ H.C. Shankar,⁴³ R.K. Shivpuri,¹³ M. Shupe,²
 J.B. Singh,³⁴ V. Sirotenko,³⁰ W. Smart,¹⁴ A. Smith,² R.P. Smith,¹⁴ R. Snihur,³¹ G.R. Snow,²⁷
 J. Snow,³³ S. Snyder,⁴ J. Solomon,¹⁷ P.M. Sood,³⁴ M. Sosebee,⁴⁴ M. Souza,¹⁰ A.L. Spadafora,²²
 R.W. Stephens,⁴⁴ M.L. Stevenson,²² D. Stewart,²⁴ D.A. Stoianova,³⁵ D. Stoker,⁸ K. Streets,²⁸
 M. Strovink,²² A. Sznajder,¹⁰ P. Tamburello,²³ J. Tarazi,⁸ M. Tartaglia,¹⁴ T.L. Taylor,³¹
 J. Thompson,²³ T.G. Trippe,²² P.M. Tuts,¹² N. Varelas,²⁵ E.W. Varnes,²² P.R.G. Virador,²²
 D. Vititoe,² A.A. Volkov,³⁵ A.P. Vorobiev,³⁵ H.D. Wahl,¹⁵ G. Wang,¹⁵ J. Warchol,³² G. Watts,⁵
 M. Wayne,³² H. Weerts,²⁵ A. White,⁴⁴ J.T. White,⁴⁵ J.A. Wightman,¹⁹ J. Wilcox,²⁹ S. Willis,³⁰
 S.J. Wimpenny,⁹ J.V.D. Wirjawan,⁴⁵ J. Womersley,¹⁴ E. Won,³⁹ D.R. Wood,²⁹ H. Xu,⁵
 R. Yamada,¹⁴ P. Yamin,⁴ C. Yanagisawa,⁴² J. Yang,²⁸ T. Yasuda,²⁹ P. Yepes,³⁷ C. Yoshikawa,¹⁶
 S. Youssef,¹⁵ J. Yu,¹⁴ Y. Yu,⁴¹ Q. Zhu,²⁸ Z.H. Zhu,³⁹ D. Zieminska,¹⁸ A. Zieminski,¹⁸
 E.G. Zverev,²⁶ and A. Zylberstejn⁴⁰

¹Universidad de los Andes, Bogotá, Colombia

²University of Arizona, Tucson, Arizona 85721

³Boston University, Boston, Massachusetts 02215

⁴Brookhaven National Laboratory, Upton, New York 11973

⁵Brown University, Providence, Rhode Island 02912

⁶Universidad de Buenos Aires, Buenos Aires, Argentina

⁷University of California, Davis, California 95616

⁸University of California, Irvine, California 92717

⁹University of California, Riverside, California 92521

¹⁰LAFEX, Centro Brasileiro de Pesquisas Fisicas, Rio de Janeiro, Brazil

- ¹¹CINVESTAV, Mexico City, Mexico
¹²Columbia University, New York, New York 10027
¹³Delhi University, Delhi, India 110007
¹⁴Fermi National Accelerator Laboratory, Batavia, Illinois 60510
¹⁵Florida State University, Tallahassee, Florida 32306
¹⁶University of Hawaii, Honolulu, Hawaii 96822
¹⁷University of Illinois at Chicago, Chicago, Illinois 60607
¹⁸Indiana University, Bloomington, Indiana 47405
¹⁹Iowa State University, Ames, Iowa 50011
²⁰Korea University, Seoul, Korea
²¹Kyungseong University, Pusan, Korea
²²Lawrence Berkeley National Laboratory and University of California, Berkeley, California 94720
²³University of Maryland, College Park, Maryland 20742
²⁴University of Michigan, Ann Arbor, Michigan 48109
²⁵Michigan State University, East Lansing, Michigan 48824
²⁶Moscow State University, Moscow, Russia
²⁷University of Nebraska, Lincoln, Nebraska 68588
²⁸New York University, New York, New York 10003
²⁹Northeastern University, Boston, Massachusetts 02115
³⁰Northern Illinois University, DeKalb, Illinois 60115
³¹Northwestern University, Evanston, Illinois 60208
³²University of Notre Dame, Notre Dame, Indiana 46556
³³University of Oklahoma, Norman, Oklahoma 73019
³⁴University of Panjab, Chandigarh 16-00-14, India
³⁵Institute for High Energy Physics, 142-284 Protvino, Russia
³⁶Purdue University, West Lafayette, Indiana 47907
³⁷Rice University, Houston, Texas 77251
³⁸Universidade Estadual do Rio de Janeiro, Brazil
³⁹University of Rochester, Rochester, New York 14627
⁴⁰CEA, DAPNIA/Service de Physique des Particules, CE-SACLAY, France
⁴¹Seoul National University, Seoul, Korea
⁴²State University of New York, Stony Brook, New York 11794
⁴³Tata Institute of Fundamental Research, Colaba, Bombay 400005, India
⁴⁴University of Texas, Arlington, Texas 76019
⁴⁵Texas A&M University, College Station, Texas 77843

We describe a search for a new heavy particle X and a W boson produced in a coherent reaction, $p\bar{p} \rightarrow W + X$. This reaction is a feature of many models including the standard model prediction of $p\bar{p} \rightarrow W^\pm H^0$, the production of the Higgs bosons of supersymmetry and various technicolor models. None of these reactions has been observed, so cross sections are based purely on theoretical expectations, which range roughly from 0.1 pb to 10 pb depending on the model. The most studied scenario is associated production of Higgs bosons (H). Although the limits on the number of allowed signal events presented in this analysis are model independent, we derive cross section limits using acceptances derived for the case in which X has the spin and decay properties of a neutral Higgs boson decaying exclusively to $b\bar{b}$.

We use events in which the W decays via $W \rightarrow l\bar{\nu}_l$, $l = e, \mu$, and the X decays as $X \rightarrow b\bar{b}$. To reduce backgrounds from W +jets in which the jets arise from gluon radiation, we require events to have a soft muon tag. The dominant source for such muons is heavy flavor decays.

In an ideal detector, the detected final state would include the charged lepton and neutrino from the W decay and a pair of jets arising from the fragmentation of the pair of b quarks.

The event selection is guided by this topology. Events are selected by requiring one high- p_T isolated lepton, significant missing energy arising from the undetected ν , and at least two central jets one of which must be tagged with a soft muon.

This analysis uses the complete DØ 1992-1995 data sample. This data has an integrated luminosity of 100 pb^{-1} and was taken at a center-of-mass energy of 1.8 TeV. The DØ detector is a general purpose detector used at the Fermilab Tevatron $p\bar{p}$ collider. It is described in detail elsewhere (1).

This paper begins with detailed descriptions of the W +jets event selection and the Monte Carlo samples used. The background analysis is then described and the cross section limits are presented. We derive the cross section limits both from a simple counting experiment comparing the number of observed and predicted events and from a fit to the mass spectrum of jets found in the events.

I. EVENT SELECTION

The base event sample for this search uses clean events having a high- p_T electron and missing transverse energy or a high- p_T muon and at least one jet. This is the same sample used in the DØ top search in the lepton plus jets channel (2). The following requirements are used to select the $W \rightarrow e\nu$ +dijet sample used in this analysis:

- Trigger
 - ≥ 1 isolated electromagnetic object $E_T \geq 20 \text{ GeV}$
 - transverse missing energy $\cancel{E}_T \geq 15 \text{ GeV}$
- One isolated e , $p_T \geq 25 \text{ GeV}$, $|\eta| < 2.5$
- Total missing transverse energy, $\cancel{E}_T \geq 25 \text{ GeV}$
- ≥ 2 jets, $|\eta| \leq 2.0$, $p_T \geq 15 \text{ GeV}$

and the $W \rightarrow \mu\nu$ sample:

- Trigger
 - ≥ 1 loose muon $p_T \geq 10 \text{ GeV}$, and
 - ≥ 1 jct, $E_T \geq 12 \text{ GeV}$, $|\eta| < 2.0$
- One isolated μ , $p_T \geq 20 \text{ GeV}/c$, $|\eta| < 1.7$
- transverse missing energy, $\cancel{E}_T \geq 20 \text{ GeV}$
- ≥ 2 jets, $|\eta| \leq 2.0$, $p_T \geq 15 \text{ GeV}$
- $p_T^W \geq 20 \text{ GeV}$
- The \cancel{E}_T is required to be isolated from the leading μ .
- The χ^2 probability from kinematic fit to the $Z^0 \rightarrow \mu^+\mu^-$ hypothesis must satisfy $P(\chi^2) \leq 0.01$.

The lepton identification is defined elsewhere (2). The isolated lepton identification has a 30% – 40% efficiency for leptons from W decay with the variation depending on the jet multiplicity and electron and muon relative inefficiencies. Jets are found using a cone algorithm with a radius of $R = 0.5$ in (η, ϕ) space. The energy of jets having an associated tag muon is defined as the vector sum of the energy measured in the calorimeter and the tag muon momentum. Details motivating the “ W -event” selection can be found in the $D\bar{O}$ top physics papers (2).

After selecting the basic W +dijet sample, the events are subdivided based on the presence and absence of a muon having $p_T \geq 4$ GeV satisfying $R \leq 0.5$. Here R is the distance in (η, ϕ) space between the muon and the closest 0.5 cone jet having $p_T \geq 15$ GeV. Such muons are produced dominantly by the decay of heavy quarks. The tag muon identification criteria are described in detail elsewhere (2). Table 1 gives a summary of the integrated luminosity and total event counts for the e +dijet and μ +dijet samples. The luminosity error is 5.4%. The search presented here uses the tagged events.

	Channel	
	e +jets	μ +jets
Integrated Luminosity (pb^{-1})	94.8	100.1
Number of Non-tagged events	1387	526
Number of tagged events	12	15

TABLE 1. Summary of luminosity and event counts for the W +dijet modes.

II. MONTE CARLO DATA

Monte Carlo is used in this analysis in the computation of the signal acceptance as a function of X mass. Simulated $p\bar{p} \rightarrow W H^0$ events were generated using the Pythia event generator (3) with the CTEQ-2M parton distribution functions (4). The (Standard Model) Higgs boson was allowed to decay according to its expected branching ratios, but only those events with $H \rightarrow b\bar{b}$ are used for this analysis. The events were processed through a full detector simulation and reconstructed with the standard $D\bar{O}$ reconstruction program. Correction factors derived by comparing data and Monte Carlo control samples were applied to the lepton identification efficiencies in simulated events where necessary.

We have also used simulated $p\bar{p} \rightarrow t\bar{t}$ events. The events were generated with the Isajet generator (5) using a top mass of 180 GeV. The detector simulation and event reconstruction processing was performed as for the signal Monte Carlo samples.

The various Monte Carlo data sets are summarized in Table 2. The $p\bar{p} \rightarrow W H^0$ cross sections are those returned by the event generator. The $p\bar{p} \rightarrow t\bar{t}$ cross section is the $D\bar{O}$ measured value of 5.2 ± 1.8 pb (2), not the result from a simulation. In all cases, the trigger efficiencies are based on measured trigger behaviour.

III. BACKGROUND

The backgrounds relevant to this search are (a) W +jets events in which the jets arise from gluon radiation, (b) multi-jet events in which fluctuations give rise to misidentification

Source	Cross Section(pb)
$WH^0, M_H = 80$ GeV	0.41
$WH^0, M_H = 90$ GeV	0.28
$WH^0, M_H = 100$ GeV	0.20
$WH^0, M_H = 110$ GeV	0.14
$WH^0, M_H = 120$ GeV	0.10
$t\bar{t}$	5.2 ± 1.8

TABLE 2. Monte Carlo samples used in this analysis and the corresponding generated cross sections. The DØ measured $p\bar{p} \rightarrow t\bar{t}$ cross section of 5.2 ± 1.8 pb is used in the analysis.

of jet systems as leptons and (c) $p\bar{p} \rightarrow t\bar{t}$ events.

The W +jets background is computed by assuming that the 1913 non-tagged W +dijet events arise from W production. The jets in these events are convoluted with a universal, flavor-blind jet tag rate function to determine the overall background after tagging. The tag rate is derived from multi-jet data and is a function of jet p_T and η . The method has been tested by applying the tag rate to untagged events in a variety of data control samples. The resulting predicted number of tagged events is compared to the observed number of tagged events sample-by-sample. The resulting differences are used to determine the systematic error. The average event tag probability for events having jet p_T and η spectra similar to those in W events is approximately 0.4%/jet. The systematic error is 0.06%/jet.

The multi-jet background arises for the electron channel when a jet fragments such that it is misidentified as an electron, and for the muon channel when a jet with a tag muon fluctuates such that the jet falls below reconstruction thresholds and the muon thus appears to be isolated. The background in both cases is computed by selecting events which satisfy all analysis criteria except the full lepton identification. For the e +jets analysis the electron criteria are relaxed to the point that the “electrons” are dominantly jets with a high electromagnetic component, and for the μ +jets channel the high- p_T muon isolation criterion is inverted giving a sample of non-isolated muons. The resulting samples are dominated by events arising from multi-jet production. The contamination from non multi-jet sources is less than 5%. The number of events in these background samples are then multiplied by the probability that the loose electron passes the full electron identification criteria (e +jets channel) or the probability that the muon+jet system fluctuates to appear as an isolated muon (μ +jets). The misidentification probability for a jet to appear as an electron is roughly 1/2000, and for a muon/jet system to appear as an isolated muon the probability roughly ranges between 5% and 15%.²

The top and Z +jets components are computed using simulated events. The $p\bar{p} \rightarrow t\bar{t}$ cross section used is the DØ measured value. The Z +jets cross section is taken from the event generator. The events are passed through a full simulation and reconstruction as described above.

Table 3 gives the total background and each of the components for both the e +jets and μ +jets channels. One sees that the background prediction of 25.5 ± 3.3 events is completely

²The jet without a muon to isolated muon fluctuation probability is somewhat smaller than the jet to electron probability. The number used here already incorporates both the branching ratio of jets to jet+muon and the efficiency for the resulting muon to pass the 20 GeV threshold in the muon identification requirements.

consistent with the 27 events observed in the data.

Source	Channel	
	$e+dijets$	$\mu+dijets$
$W+Jets$	$8.7 \pm 0.3 \pm 1.3$	$5.2 \pm 0.2 \pm 0.8$
$Z+Jets$	negligible	$0.2 \pm 0.1 \pm 0.1$
Multi-jet	$2.0 \pm 0.1 \pm 0.4$	$2.2 \pm 0.1 \pm 0.4$
$t\bar{t}$	$4.4 \pm 0.2 \pm 1.5$	$2.8 \pm 0.2 \pm 1.0$
Total	15.1 ± 2.0	10.4 ± 1.4
Combined	25.5 ± 3.3	
Observed	12	15

TABLE 3. Expected number of events in the tagged analysis. The first error is statistical. The second is systematic. The systematic errors are detailed in Table 4. The error on the combined background assumes 100% correlation between the errors on the W and $t\bar{t}$ backgrounds.

Source	Channel							
	$e+dijets$				$\mu+dijets$			
	$W+jets$	$Z+jets$	multi-jet	$t\bar{t}$	$W+jets$	$Z+jets$	multi-jet	$t\bar{t}$
Cross-Section				33%		20%		33%
Trigger				5%		5%		3%
Lepton ID				5%		13%		13%
Tag μ ID				5%		5%		5%
Fake Method			20%				20%	
Tag Rate	15%				15%			
Energy Scale				2%		3%		2%

TABLE 4. Systematic Errors on the backgrounds to the tagged analysis. The errors are expressed as a fraction of the total for the corresponding component. (*e.g.*, The 15% error on the $W+jets$ background in the $\mu+jets$ channel represents corresponds to $5.2 * 0.15 = 0.8$ events.) The W tag rate and $t\bar{t}$ cross section errors are assumed to be 100% correlated between the $e+jets$ and $\mu+jets$ channels. All others are taken to be uncorrelated.

IV. ACCEPTANCE

The acceptance for $p\bar{p} \rightarrow WH^0$ production is calculated from the simulated events described in section II above. All analysis requirements are applied to the events. The trigger efficiency is derived using data-based E_T dependence, and lepton identification corrections of between 10% and 20% are applied to the simulated events. These corrections are derived by comparing lepton identification quantities in control samples of data and simulated events. The resulting acceptances are given in Table 5. The individual components of the systematic errors are given in Table 6. The efficiencies in addition to the lepton identification discussed above are approximately 85% for the trigger efficiencies, 25% for the dijet

for a series of 50,000 simulated experiments. Here N_o is the number of events observed in the data, B is the predicted number of background events, A is the acceptance and L is the total luminosity. The 50,000 Monte Carlo experiments are generated assuming normally distributed values for N_o , B , A and L with the central values and standard deviations taken from Tables 1, 3 and 5. Events with negative cross sections are discarded. The resulting limits are given in Table 7. They range from 49 pb to 28 pb for masses from 80 GeV to 120 GeV respectively.

X Mass	$\sigma \cdot \text{Br}$ (pb) Central Value	$\sigma \cdot \text{Br}$ (pb) Limit
80	7 ± 24	49
90	6 ± 20	42
100	5 ± 17	36
110	4 ± 16	34
120	3 ± 14	28

TABLE 7. Cross section limits for the tagged analysis derived using the counting method.

B. Results from Fits to the Dijet Mass Spectrum

Limits on production of X particles are also derived by fitting the observed dijet mass spectrum to a combination of signal and background. For the tagged analysis, the two jets used to form the dijet mass are the tagged jet, and the highest E_T untagged jet.³ The resulting spectrum is shown in Fig. 1 for the data. Also shown is the predicted background derived as described above, and a fit to the background using a falling exponential with a lower mass cut off convoluted with a gaussian resolution function. The fit parameters are the mass cut off, the gaussian width and the exponential scale factor.

Figure 2 shows dijet mass spectra for $H \rightarrow b\bar{b}$. Spectra are shown for Higgs having masses of 80 and 120 GeV. The signal shape input to the limit fits is determined by fitting the dijet mass spectra in Fig. 2 to a template form. This is then normalized to unit area, and the only free parameter in the limit fits relating to the signal is the number of signal events. The template function is the sum of two exponential-gaussian convolutions of the form used for the background fit.

In the absence of initial- and final-state radiation, the dijet mass spectrum is gaussian with the width dominated by the detector resolution. Final state radiation (FSR) causes the mass of the leading two jets to decrease because of energy carried away by the FSR. Thus, the pure gaussian shape develops a tail to lower dijet masses. We assume the energy distribution of the FSR is exponentially falling. The shape of the mass distribution for the case in which both jets are from the X decay is therefore an exponential convoluted with a gaussian with the exponential falling off toward lower dijet masses.

Initial state radiation (ISR) can cause dijet pairs to be formed in which one of the jets is not from the X decay. We assume that ISR has an exponentially decreasing energy spectrum peaked at zero. The shape describing masses formed by one ISR jet and one X jet is thus assumed to peak at zero and fall off exponentially with increasing dijet mass. The

³The double tag probability is less than 1% for masses and tag efficiencies in the analysis.

Tagged Data

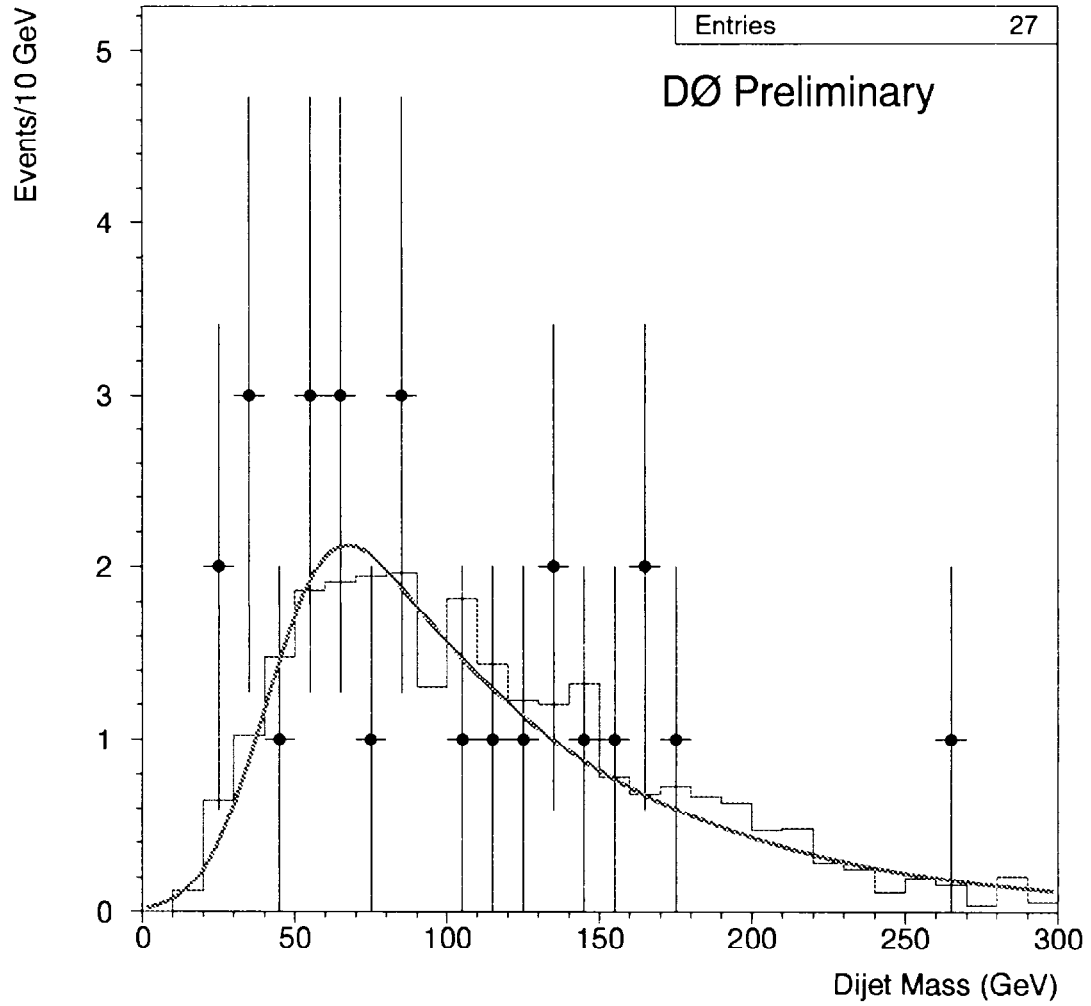


FIG. 1. Dijet mass spectrum for collider events having at least one jet with a soft muon tag. The data are the points. The histogram is the background prediction, and the curve is a fit to the background. The fit is an exponential convoluted with a gaussian.

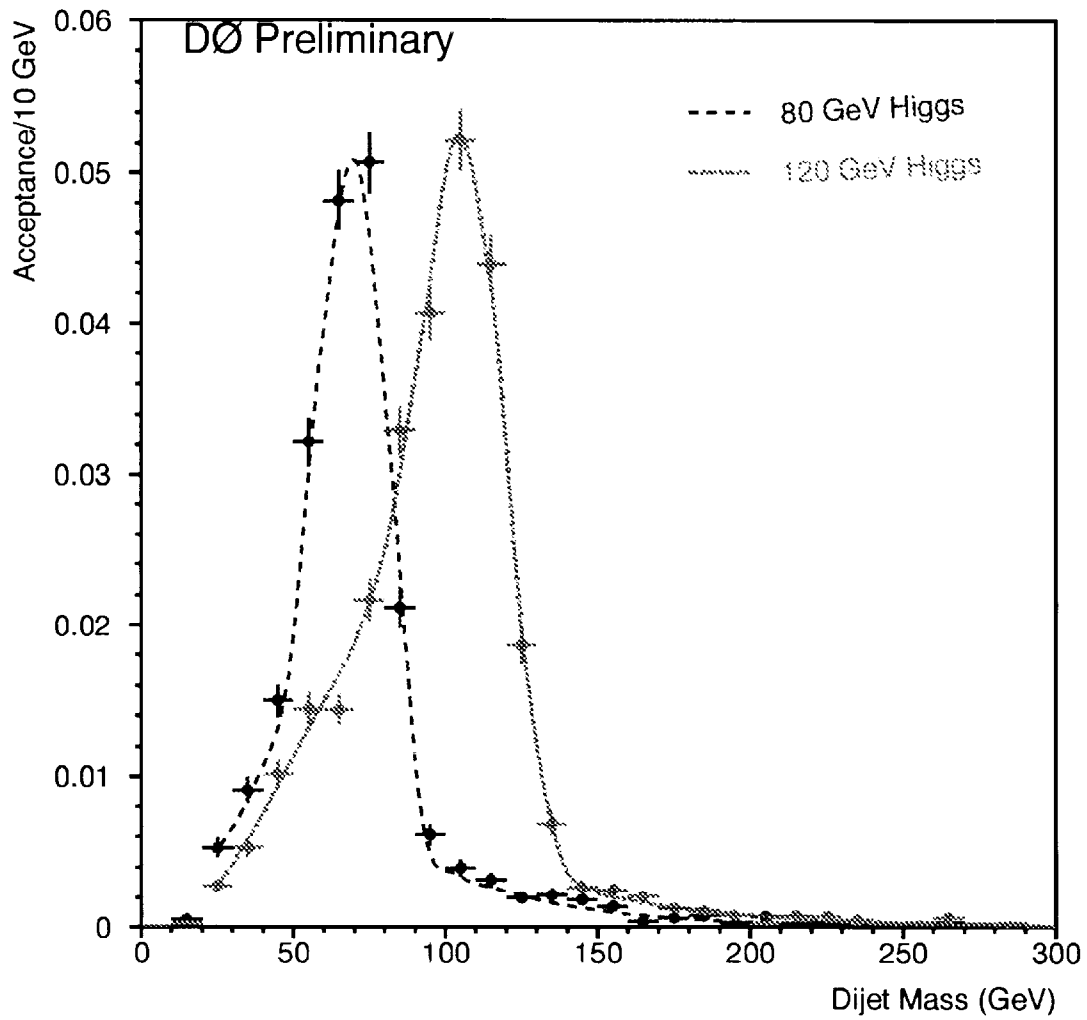


FIG. 2. Dijet mass spectrum for the signal. The spectrum is shown for Higgs bosons of 80 GeV and 120 GeV. The histograms are the results from simulated events, and the curves are the results of the fits described in the text.

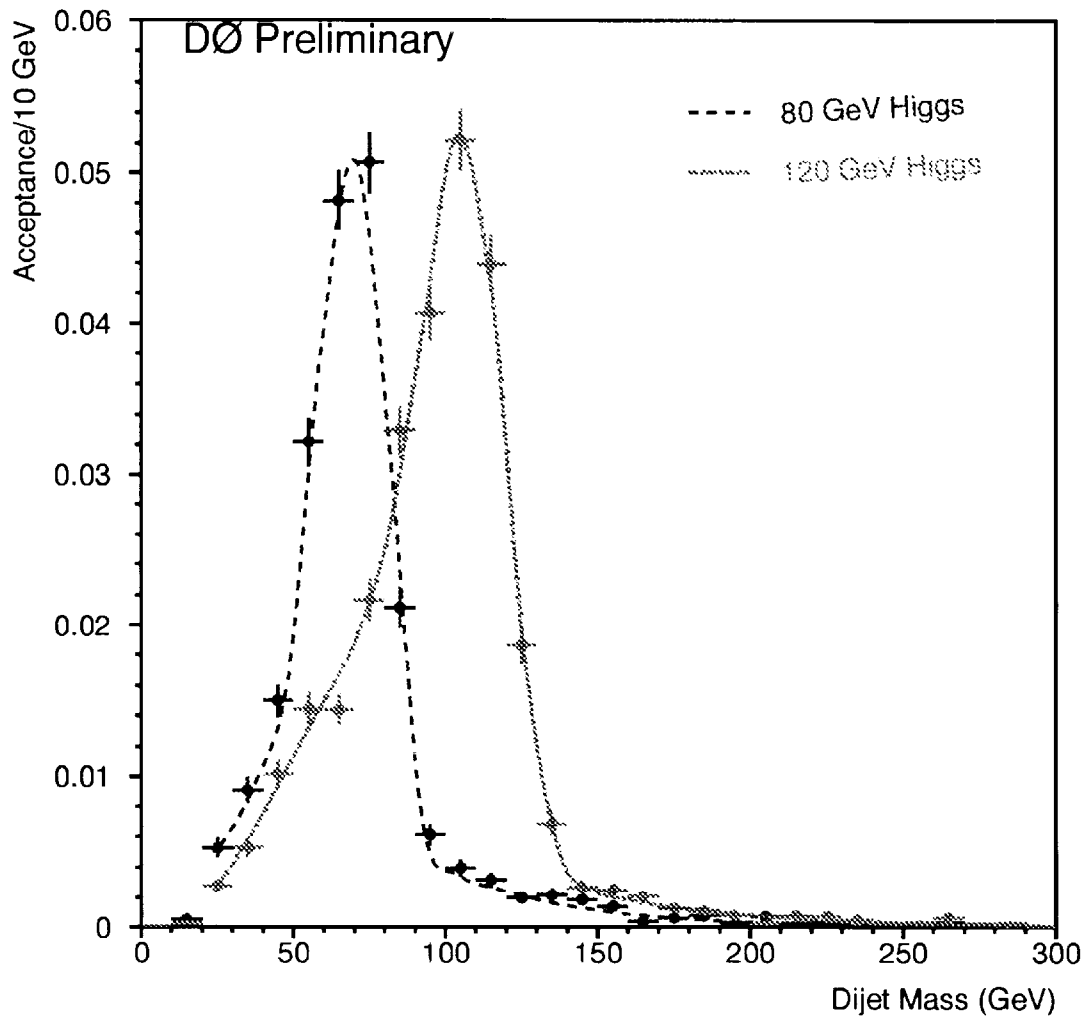


FIG. 2. Dijet mass spectrum for the signal. The spectrum is shown for Higgs bosons of 80 GeV and 120 GeV. The histograms are the results from simulated events, and the curves are the results of the fits described in the text.

selection thresholds and detector resolution impose a lower bound on the allowed masses, so the shape of the mass distribution for the case in which one jet is from ISR and the second from the X decay is an exponential convoluted with a gaussian resolution. The exponential falls off toward higher dijet masses and has a cut off at roughly 30 GeV corresponding to the jet requirement.

The signal shape s is thus defined as

$$s(M; M_0, \sigma, \alpha, M'_0, \sigma', \alpha', f) = (1 - f) \left[\int_0^\infty F(M_0 - M', -\alpha, M_0) e^{((M_0 - M)/(\sqrt{2}\sigma))^2} / \sqrt{2\pi}\sigma \right] \\ + f \left[\int_0^\infty F(M', \alpha', M'_0) e^{((M - M')/(\sqrt{2}\sigma'))^2} / \sqrt{2\pi}\sigma' \right].$$

Here M is the dijet mass and σ is the gaussian resolution for the term corresponding events in which both jets arise from the X decay. The function F is an exponential defined to be identically zero for masses $M \leq M_0$ and which has the scale factor α . The parameters M'_0 , σ' and α' correspond to the mass cut off, resolution and exponential scale factor for events in which one jet is from ISR and the other from the X decay. Finally, f is the fraction of events in which one jet is ISR and the second is from the X decay. The mass input to the exponential is $(M - M_S)/M_S$ in which M_S is a scale mass arbitrarily set to 100 GeV. It is used to avoid numerical instability in the fits arising from floating point imprecision. The combined signal shape function is illustrated in Fig. 3 with the ISR and FSR terms overlaid as separate curves.

This model is a phenomenological description, and the parameters are derived by fitting the spectra in Fig. 2 to this template form. The parameters resulting from these fits are given in Table 8 and the corresponding line shapes are shown superposed on the spectra in Fig. 2.

Parameter	Input Mass (GeV)				
	80	90	100	110	120
M_0	80.43 ± 0.55	88.78 ± 0.34	98.78 ± 0.55	106.17 ± 1.00	115.40 ± 4.15
α	4.92 ± 0.30	5.38 ± 0.32	5.87 ± 0.42	7.92 ± 1.06	6.48 ± 3.32
σ	6.65 ± 0.62	8.37 ± 0.57	8.36 ± 0.48	9.86 ± 1.09	10.87 ± 2.59
M'_0	50.22 ± 29.67	55.10 ± 5.42	46.33 ± 2.51	49.56 ± 1.27	44.13 ± 4.59
α'	2.45 ± 0.13	2.84 ± 0.17	2.35 ± 0.14	2.87 ± 1.03	2.14 ± 0.12
σ'	0.75 ± 48.70	22.44 ± 4.17	18.36 ± 2.63	21.75 ± 1.47	17.94 ± 3.60
f	0.26 ± 0.14	0.28 ± 0.05	0.34 ± 0.03	0.43 ± 1.03	0.34 ± 0.02
χ^2/dof	31/19	22/21	15/21	31/19	31/21

TABLE 8. Parameters for signal dijet mass shapes. The parameters were derived by fitting samples before applying the tag criterion. Kolmogorov-Smirnov tests indicated little statistical difference between the tagged and non-tagged shapes.

The function used in performing the final fits is thus

$$f(M; N_S, N_B, \alpha, M_0^B, \sigma) = N_S * s(M) + N_B * b(M; \alpha, M_0^B, \sigma).$$

Here, N_S is the number of signal events, N_B is the number of background events and α , m_0^B and σ_B are the parameters for the background shape function. The function is fit to the data spectrum using a χ^2 minimization.

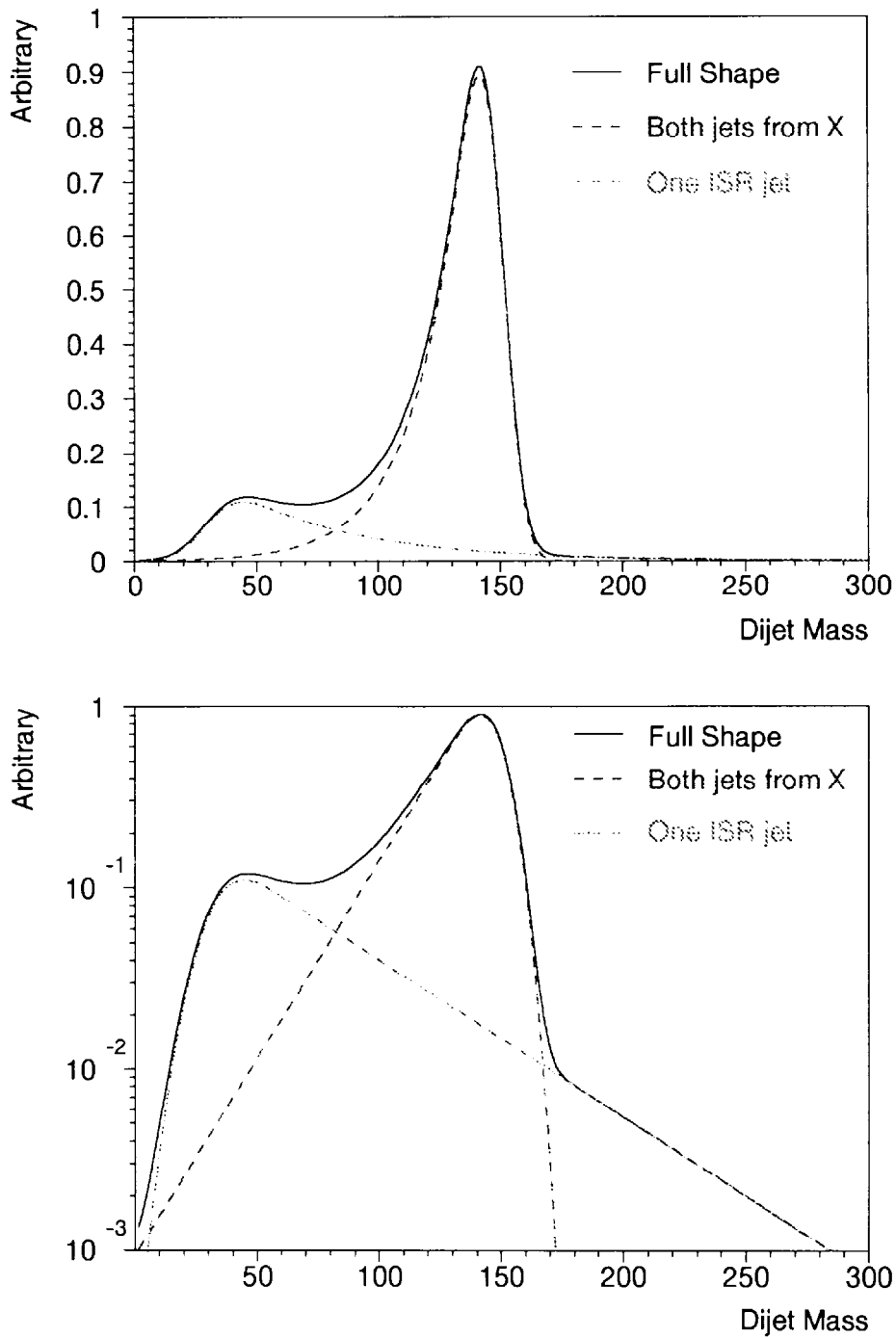


FIG. 3. Illustration of the signal dijet mass distribution template function.

These background and signal shapes are used as the input spectra for a single-parameter binned maximum likelihood fit. The fit parameter is the fraction of $W^\pm H^0$ signal in the data. The likelihood function is

$$L = \prod_i P(N_i; \mu_i).$$

Here P is the Poisson probability of finding N_i data events in the i -th mass bin of Fig. 1 when the average expected is $\mu_i = N[f_i^B(1 - \alpha) + f_i^S\alpha]$. The parameters f_i^B and f_i^S are respectively the fraction of background and signal which fall in the i -th mass bin, and α is the fraction of the events in the total sample arising from $p\bar{p} \rightarrow WH^0$. The total number of observed events is denoted N . The fractions f_i^B and f_i^S are taken from the parametrized background and signal shapes. Table 9 shows the results of blind tests of the fitting procedure.

Input Parameters			Fit Results			
M_H (GeV)	N_B	N_S	N'_B	N'_S	X Fraction	
120	15	21	20 ± 7	16 ± 7	0.4 ± 0.2	
120	25	3	$28^{+0}_{-2.5}$	$0.0^{+2.5}_{-0.0}$	$0.0^{+0.09}_{-0.0}$	
120	3	24	$0.0^{+4.3}_{-0.0}$	$27^{+0.0}_{-4.3}$	$1.0^{+0.0}_{-0.16}$	
80	13	15	11 ± 5	17 ± 5	$0.6^{+0.2}_{-0.6}$	
80	19	4	15 ± 4	8 ± 4	0.34 ± 0.18	

TABLE 9. Blind tests of the fitting method used in the tagged analysis.

Table 10 shows the fitted fraction of $p\bar{p} \rightarrow WH^0$ events in the tagged data sample. Also shown is the corresponding number of $p\bar{p} \rightarrow WH^0$ events. The error is the statistical error found by varying the fraction until the log likelihood changes by one half unit. The likelihood functions are shown in Fig. 4.

X Mass (GeV)	α (%)	N_H	$\sigma * Br$ (pb)	$\sigma * Br$ Limit (pb)
80	$13.9^{+20.9}_{-13.9}$	$3.8^{+5.8}_{-3.8}$	3^{+5}_{-3}	52
90	$3.6^{+22.6}_{-3.6}$	$1.0^{+6.1}_{-1.0}$	1^{+5}_{-1}	40
100	0^{+12}_{-0}	$0^{+3.3}_{-0}$	0^{+3}_{-0}	28
110	$0^{+8.5}_{-0}$	$0^{+2.3}_{-0}$	0^{+2}_{-0}	25
120	$0^{+7.8}_{-0}$	$0^{+2.1}_{-0}$	0^{+2}_{-0}	19

TABLE 10. Results for the tagged analysis likelihood fit. The parameter α is the fraction of data attributed to $p\bar{p} \rightarrow WH^0$. N_H is the number of events attributed to $p\bar{p} \rightarrow WH^0$. For all masses, the answer is consistent with zero. The column labelled “ $\sigma * Br$ Limit” gives the 95% confidence upper bounds on the production of $p\bar{p} \rightarrow WH^0$.

Limits on the production cross section are derived by generating 50,000 experiments with weights for the number of signal events derived according to the likelihoods, and for the acceptance and luminosities derived from normal distributions with the means and

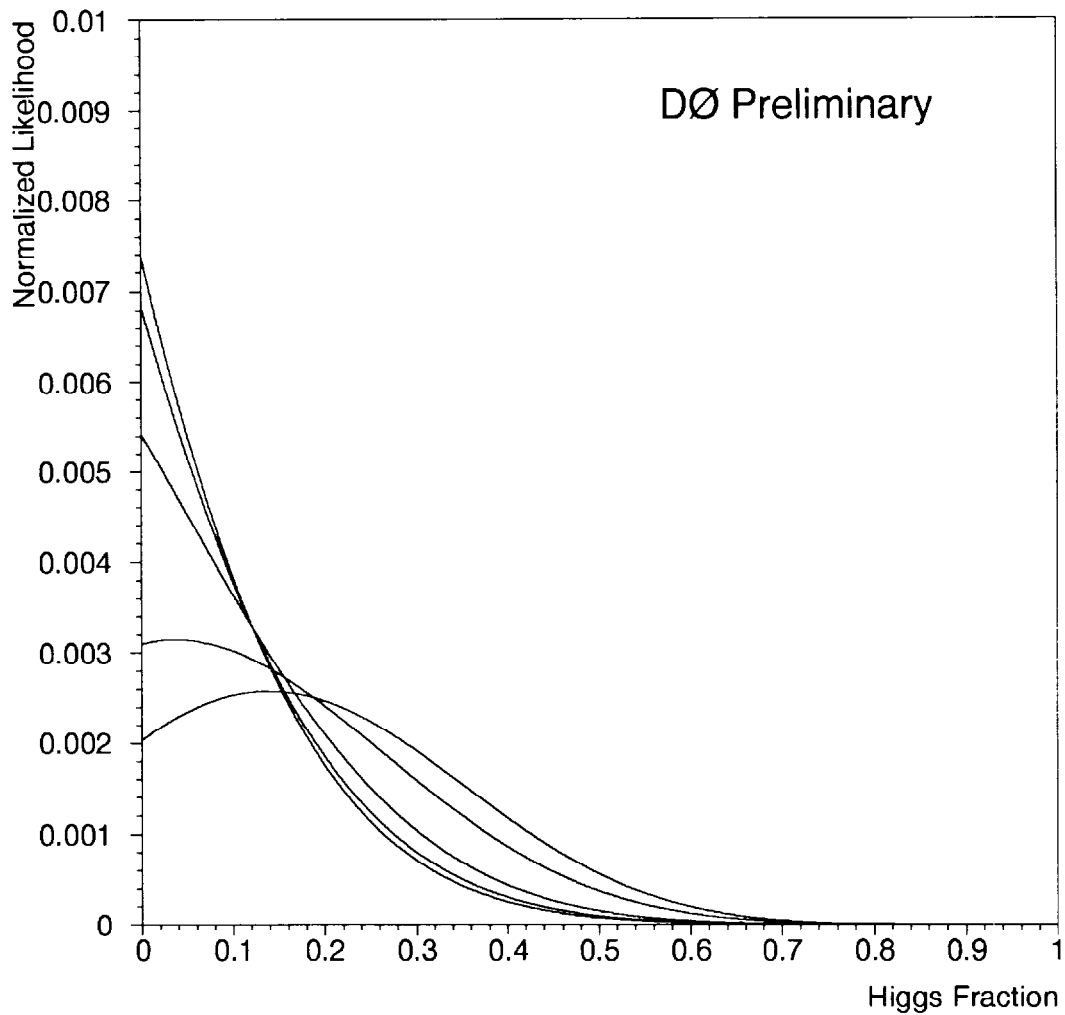


FIG. 4. The likelihoods resulting from the shape fit used in the mass-fit analysis. The horizontal axis is the X fraction α and the areas are normalized to unity. The curves are for X masses of 80, 90, 100, 110 and 120 GeV. The original likelihoods can be found by multiplying these curves by 7770, 6310, 3740, 2350 and 2730 for masses of 80, 90, 100, 110 and 120 GeV respectively. The curve extending to the highest X fraction corresponds to $M = 80$ GeV. The trend to lower fractions is monotonic as a function of X mass.

deviations given above. Experiments giving a negative cross section are discarded. The 95% confidence limits are derived by numerical integration of the weights and are shown in Table 10 and in Fig.5. The limits range from 52 pb to 19 pb for X masses from 80 GeV to 120 GeV.

VI. CONCLUSIONS

We have searched for evidence of a massive state decaying to a pair of b quarks which is produced in association with a W boson. The data and predicted background levels agreed, and cross section limits were set using two methods. The first was a simple counting experiment, and the second used the shape of the dijet mass spectrum input to a likelihood fit. Preliminary cross section limits ranging from 20 pb at a mass of 120 GeV to 60 pb at a mass of 80 GeV are set.

ACKNOWLEDGMENTS

We thank the staffs at Fermilab and the collaborating institutions for their contributions to the success of this work, and acknowledge support from the Department of Energy and National Science Foundation (U.S.A.), Commissariat à l'Énergie Atomique (France), Ministries for Atomic Energy and Science and Technology Policy (Russia), CNPq (Brazil), Departments of Atomic Energy and Science and Education (India), Colciencias (Colombia), CONACyT (Mexico), Ministry of Education and KOSEF (Korea), CONICET and UBACyT (Argentina), and the A.P. Sloan Foundation.

REFERENCES

- * Visitor from IHEP, Beijing, China.
 - † Visitor from Univ. San Francisco de Quito, Ecuador.
1. Abachi, *et. al.*, Nucl. Instrum. Methods A **338**, 185 (1994).
 2. Abachi, *et. al.*, Phys. Rev. D, **52**, 4877.
and updated in M. Narain (for the $D\bar{D}$ collaboration), presented at Les Rencontres de Physique de La Vallée D'Aoste, La Thuile, Italy (Mar. 1996).
 3. T. Sjostrand, Computer Physics Commun. **82** 74 (1994).
 4. H. L. Lai, *et. al.*, Phys. Rev. D **51**, 4763 (1995).
 5. F. Paige and S. protopopescu, BNL Report No. BNL38034, 1986 (unpublished), release 7 00.

Tagged Analyses, Cross Section Results

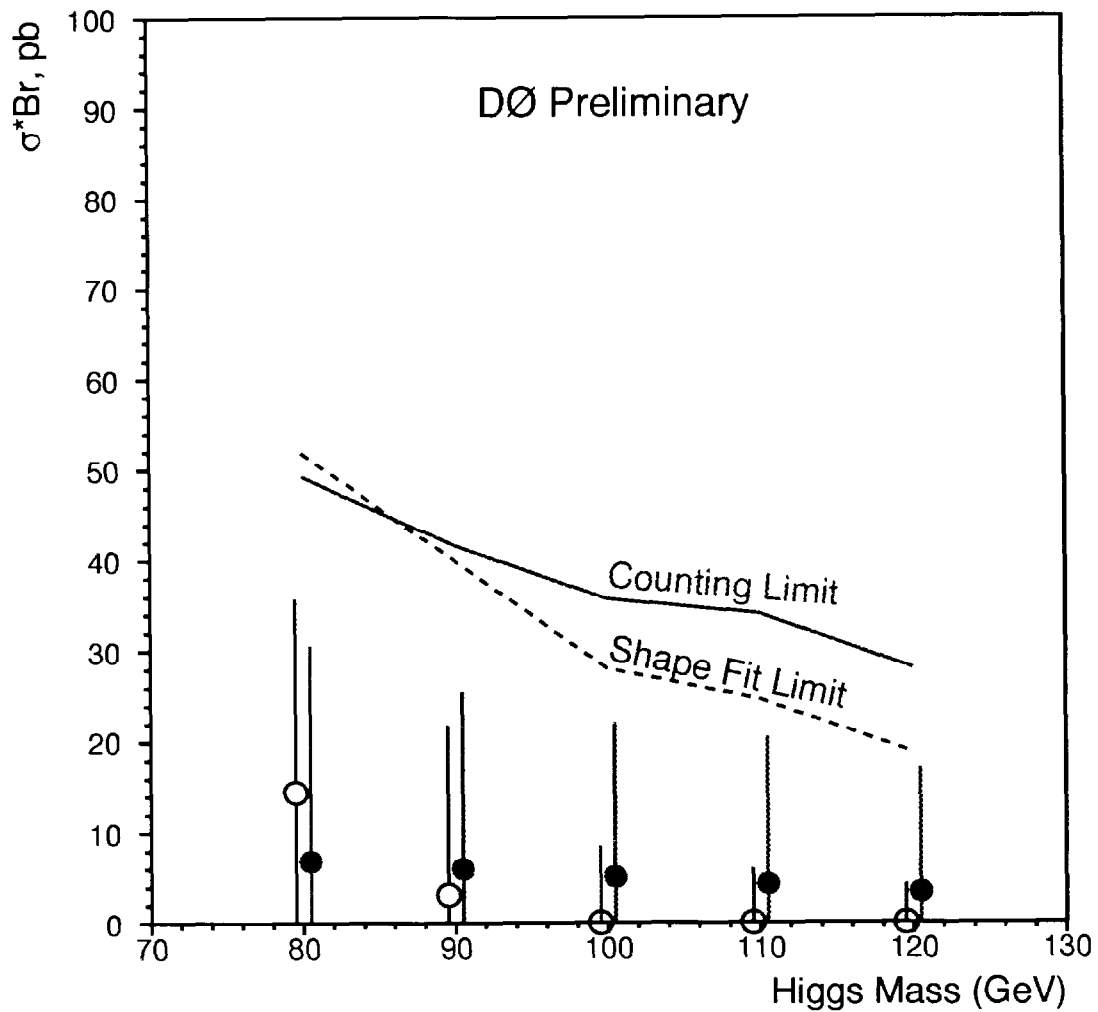


FIG. 5. The $\sigma * Br$ results for the tag analyses. The open circles are the central values for the shape fit result and the dashed line is the 95% confidence upper bound. The solid circles and solid lines are the central value and upper bound for the counting experiment results.